Structural Organization of the Receptor Associated Protein†

Ana Lazic,‡,§ Klavs Dolmer,‡,§ Dudley K. Strickland,|| and Peter G. W. Gettins*,§

Department of Biochemistry and Molecular Genetics, College of Medicine, University of Illinois at Chicago, Chicago, Illinois 60607-7170, and Department of Vascular Biology, American Red Cross, Rockville, Maryland

Received October 2, 2003; Revised Manuscript Received October 24, 2003

ABSTRACT: The receptor associated protein (RAP) is a 38 kDa ER-resident protein that binds tightly to the low density lipoprotein receptor-related protein (LRP), and other members of the LDL receptor family of receptors, and competes with all known LRP ligands for binding to LRP. To better understand the domain structure and organization of RAP, we have expressed RAP subfragments and examined them by two-dimensional HSQC NMR and fluorescence spectroscopies, by differential scanning calorimetry, and by both equilibrium and velocity sedimentation measurements. We found that the protein is organized into three domains located in the first third (1D), middle third (2D), and last third (3D) of the protein. All three domains adopt stable tertiary structure as isolated domains and are monomers. Whereas domains 1D and 2D do not interact with one another, 3D interacts with 2D, both in a 2D-3D construct and in intact RAP. Sedimentation measurements also indicated that intact RAP, although monomeric, is significantly elongated.

The 38 kDa receptor-associated protein (RAP)[1] was first isolated as a protein that copurifies with the low-density lipoprotein receptor-related protein (LRP) and that is present in variable stoichiometry relative to LRP (*1*). The tight interaction responsible for this copurification (K_d ~3 nM) reflects the role that RAP is believed to play in vivo as a chaperone for correct folding of LRP and of certain other members of the LDL receptor family and also in preventing premature binding of protein ligands to folded LRP in the ER or Golgi (*2*−*4*). The finding that RAP competes for binding of all protein ligands of LRP (*2*, *5*−*9*) has made it an invaluable reagent for mapping LRP's ligand binding regions but raises the question of how RAP can bind at multiple sites within LRP and also compete for binding with ligands of very different primary and tertiary structures. To answer this question, it will be necessary to have an understanding of RAP's structural organization and ultimately of the atomic details of its binding to the ligand binding regions of LDL receptor family members such as LRP. To date, the only atomic resolution structural information on RAP is an NMR solution structure of residues 18−112 (out of a total of 323 residues in full-length RAP), showing it to contain a compact three helical bundle, but with residues 93−112 disordered (*10*). This domain is of functional interest in that it contains the epitope for the Heyman nephritis antigen (*11*).

Several models have been proposed for the domain organization and structure of RAP, although in each case based on relatively limited data. The first, proposed by Bu and colleagues, recognized an apparent triplication of an approximately 100 residue sequence within the primary structure of RAP and suggested that the protein is organized into three domains, one associated with each of the three repeats, although with different functions associated with each domain. A modification of this model incorporated data on sites of proteolytic susceptibility and denaturation by guanidine hydrochloride and proposed a two-domain structure, with portions of the middle repeat being associated with each of the flanking repeats, to give a total of only two domains. An independent study by Ellgaard expressed each of the three repeats as a separate peptide and used one-dimensional ^{1}H NMR and ligand binding measurements to propose a three-domain model, although without examining any domain−domain interactions in larger constructs or in intact RAP. More recently, a differential scanning calorimetry (DSC) and CD study of RAP and subfragments proposed a four-domain model, with the first and last domains corresponding approximately to those of Ellgaard and colleagues but with the middle repeat being composed of two domains, the first of which was proposed to associate with the N-terminal domain.

To more definitively determine the number and size of individual domains within RAP, and to determine whether any of them interact in the intact protein, we have used a

† The Bruker DRX600 NMR spectrometer was purchased with funds from Grant BIR-9601705 from the NSF Academic Research Infrastructure Program and matching funds from the University of Illinois at Chicago. The cryoprobe used for some of the NMR experiments was purchased with funds from NIH shared instrumentation Grant 1S10 RR15757-01. The VP-DSC was purchased with funds from NIH shared instrumentation Grant 1S10 RR15958-01. The work was supported by NIH Grants GM54414 (P.G.W.G.) and HL50784 and HL56051 (D.K.S.).

* Corresponding author. Phone: (312) 996-5534. Fax: (312) 413-0364. E-mail: pgettins@uic.edu.

‡ These authors contributed equally to the study.

§ University of Illinois at Chicago.

|| American Red Cross.

[1] Abbreviations: LRP, low-density lipoprotein receptor-related protein; RAP, receptor associated protein; DSC, differential scanning calorimetry; CD, circular dichroism; HSQC, heteronuclear single quantum coherence spectroscopy; TEV, tobacco etch virus; 1D, RAP fragment 1−112; 2D, RAP fragment 93-215; 3D, RAP fragment 206−323; 1−2D, fragment 1−215; D1, RAP fragment 1−92; D2, RAP fragment 93−163; D3, RAP fragment 164−216; D4, RAP fragment 217−323; D1−2, RAP fragment 1−164; ΔH^{cal}, measured enthalpy change; $\Delta H^{van't\ Hoff}$, van't Hoff enthalpy.

10.1021/bi035779e CCC: $25.00
Published on Web 11/22/2003

combination of two-dimensional HSQC NMR, differential scanning calorimetry, fluorescence spectroscopy, and sedimentation measurements on intact RAP and on subfragments. Our findings indicate that none of the previous models fully represents intact RAP in terms of the number of domains and/or domain−domain interactions. Instead, we found that, whereas there are 3-folded domains each representing about one-third of the protein, as found previously by Ellgaard et al. (*12*), the second and third domains interact weakly with one another, whereas the first domain is entirely independent. Furthermore, sedimentation velocity measurements showed that the domains are organized in a way that gives a significantly elongated structure, although the protein behaves as a monomer.

MATERIALS AND METHODS

Expression, Purification, and Refolding of RAP and RAP-Derived Domains. The expression vector pGEX-2T (Amersham Biosciences) containing the RAP cDNA was used as a template for construction of RAP subfragments: 1D (1−112) and 1−164, 2D (93-215), 3D (206−323), 1D-2D (1−215), and 2D-3D (93−323) in polymerase chain reactions. PCR products were cloned into either pGEX-2T or pQE30NusA-TEV expression vectors. The pGEX-2T vector was transformed into BL-21 cells, while pQE30NusATEV vector was transformed into SG13009 cells. The pGEX expression vector was designed to produce fusion proteins of the insert-encoded protein coupled to glutathione *S*-transferase (GST), with a thrombin cleavage site between them. The pQE30NusA-TEV expression vector was designed to produce fusion proteins of the insert-encoded protein coupled to 6His-NusA protein, with a TEV proteinase cleavage site between.

Fusion proteins were expressed either in *Escherichia coli* BL-21 cells in 2YT medium supplemented with 150 mg/L ampicillin or SG13009 cells in 2YT medium supplemented with 150 mg/L ampicillin and 50 mg/mL kanamycin. Expression was induced with 1 mM IPTG at an OD_{600} of 0.6. The cells were harvested by centrifugation after a further 4−5 h growth at 37 °C. For NMR experiments, cells were grown in minimal medium, consisting of M9 salts supplemented with 6 mL/L MEM vitamin solution (Gibco BRL), 1 mM $MgSO_4$, 40 μM $CaCl_2$, 2 g/L glucose, and 1 g/L $^{15}NH_4Cl$ (Cambridge Isotope Laboratories). Cells were induced as above and were harvested after 6 h.

Harvested cells with expressed GST-fusion proteins were resuspended in TBSTE buffer (20 mM Tris, 150 mM NaCl, 10 mM EDTA, 0.5% Triton X-100, 0.5%, β-mercaptoethanol (βME), pH 7.9) and sonicated for 5 min total pulse time. GST-fusion proteins were isolated from whole cell lysate by GSH-Sepharose chromatography and dialyzed overnight against 20 mM Tris, 50 mM NaCl, 4 mM EDTA, and 0.1% βME. Following cleavage with thrombin (1:5000 mol/mol ratio, 15 min at 20 °C), GST was removed from the domain of interest by GSH−Sepharose chromatography. RAP or RAP subfragments were subsequently purified by anion exchange chromatography on Q-Sepharose HP (Pharmacia) in 20 mM Tris, pH 8.0, using a linear gradient of 0−500 mM NaCl, except for full-length RAP, where the gradient was 50−500 mM due to RAP's low solubility in low salt buffers. Purified RAP and RAP subfragments were dialyzed against 20 mM Tris, 50 mM NaCl, pH 7.4.

6His-NusA-fusion proteins were purified from whole cell lysate using Ni-NTA affinity chromatography (Qiagen), according to the manufacturer's directions. After cleavage with TEV proteinase (1:1000 w/w, overnight at 4 °C), 6His-NusA was removed from the protein of interest by Ni−NTA affinity chromatography. RAP and RAP subfragments were additionally purified by the same anion exchange chromatography step that was used in the purification of GST-fusion proteins.

Protein concentrations were determined spectrophotometrically, using extinction coefficients calculated from the composition of tryptophan and tyrosine residues present in each fragment and the relationship ϵ^{280} (M^{-1} cm^{-1}) = 5500 × number of tryptophans + 1490 × number of tyrosines (*13*). The extinction coefficients determined were 13 980 M^{-1} cm^{-1} for 1D, 12 490 M^{-1} cm^{-1} for 2D, 9970 for 3D, and appropriate linear sums for other constructs or for intact RAP.

Differential Scanning Calorimetry. Experiments were performed on a MicroCal VP-DSC differential scanning calorimeter using a scan rate of 1 °C/min. Proteins were dialyzed into the same buffer as used previously by Medved et al. (*14*), namely, 20 mM glycine, 0.25 M guanidine hydrochloride, pH 8.7. Protein concentration in the cell was 1 mg/mL (~8 μM). Differential scanning calorimetric data were analyzed using MicroCal DSC−Origin, using the model of independent two-state transitions, from which T_m, ΔH^{cal}, and $\Delta H^{van't\ Hoff}$ are calculated.

NMR Spectroscopy. [$^1H^{15}N$]-HSQC spectra were recorded on a Bruker DRX600 instrument equipped with a 5 mm ($^1H/^{15}N/^{13}C$) triple resonance cryoprobe and pulse field gradient capability. Uniformly ^{15}N-labeled samples of RAP and RAP subfragments were prepared in 20 mM Tris, 50 mM NaCl, pH 7.4, 90% H_2O/10% D_2O at a protein concentration of 0.4 mM or 100 μM, while the sample of RAP run under optimal conditions for cryoprobe detection was 10 μM prepared in 50 mM MOPS buffer titrated with bis-TRIS-propane at pH 7.2. Spectra were recorded at 298 or 293 K. [$^1H^{15}N$]-HSQC data were processed and analyzed by NMRPipe (*15*).

Fluorescence Measurements. Fluorescence spectra were recorded on a QuantaMaster spectrofluorimeter (Photon Technology International, London, Ontario, Canada). Excitation was at 295 nm, to ensure excitation of only the tryptophans, with slits of 1 nm for excitation and 4 nm for emission. Emission was recorded between 305 and 400 nm in steps of 1 nm with an integration time of 1 s at 25 °C. All proteins were in 20 mM Tris, 50 mM NaCl, pH 7.4 at a concentration of 5 μM. Spectra were normalized based on the fluorescence intensity in 6 M guanidine hydrochloride and the number of tryptophans in the fragment.

Sedimentation Velocity and Sedimentation Equilibrium Measurements. Sedimentation velocity and sedimentation equilibrium experiments were performed on an XLA Beckman Coulter analytical ultracentrifuge at the Keck Biophysics Facility at Northwestern University. For sedimentation velocity measurements, RAP in the same buffer as used for the NMR experiments (20 mM Tris, 50 mM NaCl, pH 7.4), at different concentrations, was centrifuged at 60 000 rpm for several hours. Sedimentation of samples was followed by absorbance at 280 nm for the 1 mg/mL sample and at 297 nm for the 3.5 mg/mL sample to maintain an OD of about 0.9.

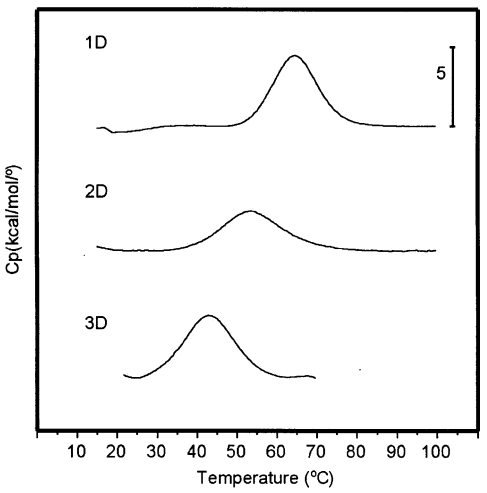

FIGURE 1: RAP unfolds as three distinct domains. DSC traces for unfolding of RAP fragments. From top to bottom the traces represent fragment 1−112 (1D), fragment 93-215 (2D), and fragment 206−323 (3D).

Table 1: Thermodynamic Parameters for Unfolding of Various RAP Constructs

species	T_m (°C)	ΔH^{cal} (kcal mol^{-1})	$\Delta H^{van't\ Hoff}$ (kcal mol^{-1})	ratio[a]
1D (1−112)	64.7	65.3	64.2	1.02
2D (93−215)	54.0	49.8	43.2	1.15
3D (216−323)	43.2	62.0	51.7	1.20

[a] Ratio represents the ratio $\Delta H^{cal}/\Delta H^{vH}$, which is a measure of how many unfolding units (domains) are present within a transition.

For sedimentation equilibrium measurements, fragments 1D, 2D, 3D, 2D-3D, and intact RAP samples were prepared in 20 mM potassium phosphate buffer, pH 7.4 containing 50 mM NaCl. Scans were collected at 25 °C at 230 and 280 nm in radial step mode, with a 0.001 cm radial resolution. Determinations were the average of 20 measurements. Three concentrations were used for each type of sample, with OD values of 0.3, 0.5, and 0.7 for both wavelengths. Samples were sedimented to equilibrium at 32 000, 38 000, 44 000, and 50 000 rpm for 1D, 2D, and 3D; at 24 100, 34 200, 41 900, and 48 300 rpm for 2D-3D; and at 18 300, 25 100, 30 400, 34 900, and 38 900 rpm for intact RAP. Data were analyzed by UltraScan II Data Analysis Software.

RESULTS

Differential Scanning Calorimetry. Using the same buffer conditions as Medved et al., DSC scans were carried out on the three constructs 1D, 2D, and 3D, representing the first, middle, and last thirds of RAP. Each species gave a simple unfolding transition that was very well-fitted to a two-state unfolding process (Figure 1). In addition, the ratio of $\Delta H^{calorimetric}/\Delta H^{van't\ Hoff}$ was 1, within experimental error (Table 1), indicating that only a single domain was present in each species. The relative stabilities of the three domains were the same as found previously for constructs that covered equivalent portions of RAP, with the T_m values being 65 °C for 1D, 54 °C for 2D, and 42 °C for 3D (*14*).

2D [^{1}H-^{15}N] HSQC NMR Spectra of RAP Fragments. The two-dimensional [^{1}H-^{15}N] HSQC NMR spectrum of the first 112 residues of RAP, expressed as a uniformly ^{15}N-enriched protein, showed excellent resolution (Figure 2A), although with a relatively small dispersion in the ^{1}H dimension (about 2 ppm excluding NH_2 side chains and indole NH), consistent with the earlier NMR structure determination of this region, which showed the presence of a three-helical bundle encompassing residues 18−88 (*10*). An HSQC NMR spectrum was also recorded of a closely related construct, residues 1−92 (spectrum not shown), which contains the whole of the ordered structure found previously. Of the 76 backbone NH resonances resolvable in the spectrum of 1−92 (out of 87 nonproline residues that are expected to give resonances), all were present at either identical positions (64 peaks) or only slightly perturbed positions (12 peaks) in the spectrum of 1−112. Furthermore, 19 additional peaks were present, out of the 20 expected for the extra residues 93−112. Almost all of the additional peaks occurred at ^{1}H chemical shifts of 8.05−8.35 ppm, indicating a random coil structure for this linker region. This is in keeping with what has been reported previously for this region, namely, that the portion 93−112 is unstructured and highly flexible as part of the fragment 18−112 (*12*).

The fragment 1−164 had been reported by Medved et al. to contain two distinct domains, one from 1 to 92 and one from 93 to 164 (*14*). The two-dimensional [^{1}H-^{15}N] HSQC NMR spectrum of this fragment (Figure 2B) consisted of all of the narrow resonances present in the spectrum of the fragment 1−112 (Figure 2A), together with additional intensity in the center of the spectrum that was broad and unresolved, implying that the additional residues from 113 to 164 did not give rise to any narrow, dispersed resonances suggestive of a new structured domain.

The fragment 93−215 gave a well-dispersed, well-resolved HSQC NMR spectrum (Figure 2C), consistent with this region also containing a well-folded domain. Approximately 70 resonances were clearly resolvable as dispersed, single peaks, although these probably include some that represent the flexible region from 93−112 that are also present in the fragment 1−112. In addition to these resonances, there is considerable broad overlapping intensity between 119 and 123 ppm (^{15}N dimension) and 8.0 and 8.4 ppm (^{1}H dimension). This suggests that some portion may be undergoing conformational interconversion and hence give broadened lines.

The fragment 206−323 gave a spectrum with a similar spread of chemical shifts in the ^{1}H dimension as the fragments 1−112 and 93−215, although with a fewer number of resonances that were completely resolved (Figure 2D). Thus, many of the resonances had ^{1}H chemical shifts at about 8 ppm, with the result that there was significant overlap in this region even though the resonances themselves were relatively narrow. Nevertheless, the spectral dispersion indicated that there was an ordered conformation within this fragment.

Independence of Domains 1D and 2D. To examine the dependence of the structure present in domain 1D on the presence of domain 2D and vice versa, the two-dimensional [^{1}H-^{15}N] HSQC NMR spectrum of the fragment 1−215 was recorded and compared with the sum of the spectra of 1−112 and 93−215. The spectrum of fragment 1−215 was well-resolved (Figure 3A) and represented a simple superpositioning of the resonances seen previously from the fragment 1−112 and the additional resonances present in the fragment 93−215 (Figure 3C). This shows that the domains present

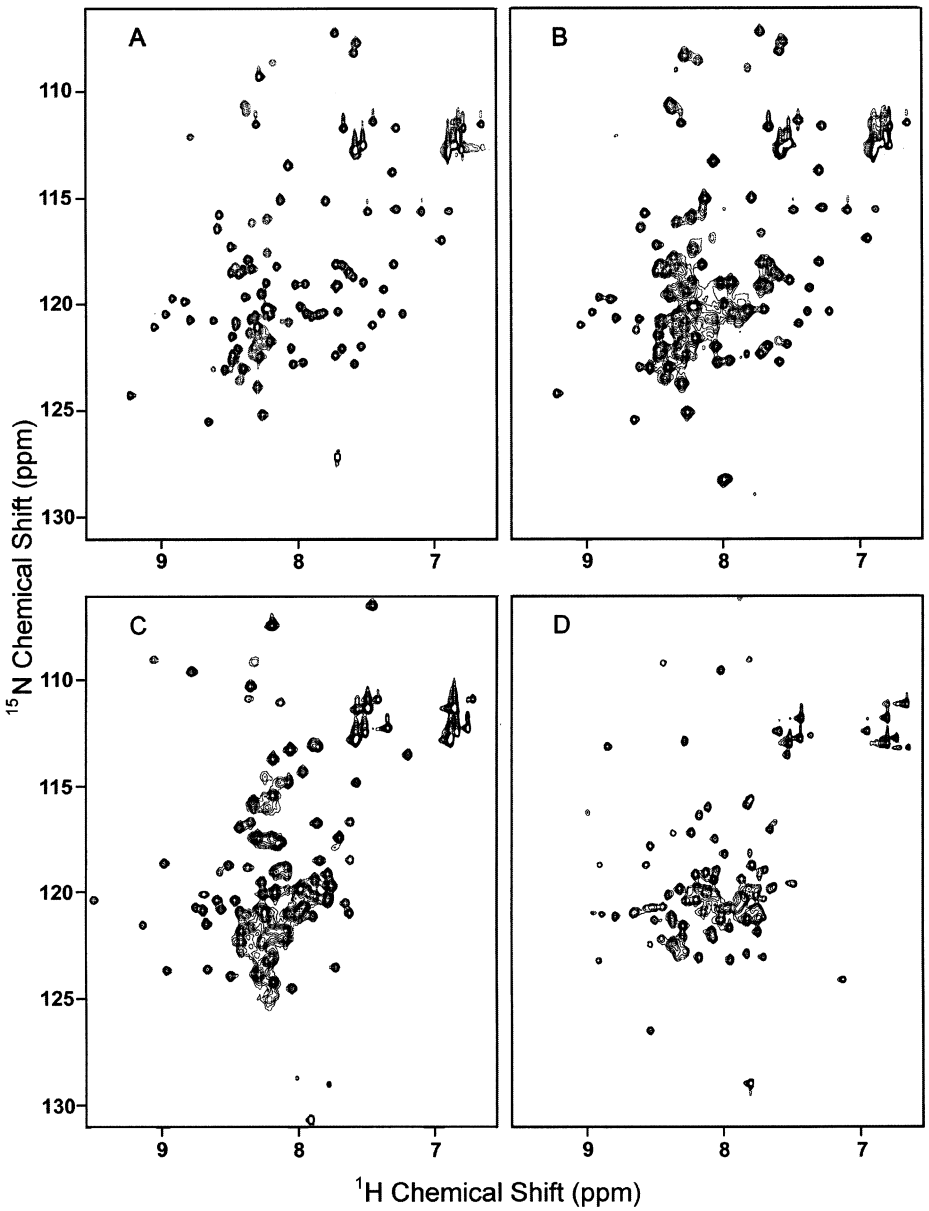

FIGURE 2: RAP contains only three discrete folded domains. [^{15}N-^{1}H]-HSQC NMR spectra of uniformly-^{15}N-labeled RAP domains recorded at 25 °C and 600 MHz for ^{1}H. Panel A, fragment 1−112, encompassing domain 1D; panel B, residues 1−164; panel C, residues 93-215 encompassing domain 2D; panel D, residues 206−323, encompassing domain 3D. Note that the very sharp resonances at ^{15}N chemical shifts of 127 ppm in panel A, 131 ppm in panel B, and 129 ppm in panel C are likely to arise from the C-terminal residue, based on their strong downfield chemical shifts and high intensity. Also, the spectra have been plotted only as far downfield as 9.5 ppm (^{1}H) and thus do not show the resonances present from tryptophan indole NHs.

in the individual fragments were also present in the longer fragment, with the same structures, suggesting that there was no domain−domain interaction between these two domains. The narrow line widths, similar to those of each of the smaller fragments, are also consistent with two independently mobile domains being present rather than a single slower moving domain, which would have resulted in much broader resonances throughout.

Interaction between Domains 2D and 3D. A similar comparison was made between the behavior of domains 2D and 3D as isolated fragments and as a single connected species by recording the two-dimensional [^{1}H-^{15}N] HSQC NMR spectrum of fragment 93−323 and comparing it to the sum of NMR spectra of the constituent separate fragments. The spectrum of 93−323 was very poorly resolved, with almost no discernible individual resonances, and most of the signal intensity occurring in the center of the spectrum around 8 ppm (^{1}H) as unresolved resonance intensity (Figure 3B). This contrasts markedly with the simple sum of spectra of the component fragments (Figure 3D) and implies that there is an interaction between the two domains that is sensed by most or all of the residues in both domains. Spectra of this tandem domain species were also recorded in the presence of higher salt concentration or of low concentrations of guanidine or detergent in an attempt to disrupt the interaction between the domains. However, none of these spectra had a significantly improved resolution that might indicate such a disruption (data not shown).

2D [^{1}H-^{15}N] HSQC NMR Spectrum of Intact RAP. Intact RAP gave an HSQC NMR spectrum composed of a set of narrow well-resolved, well-dispersed resonances and a region of broad unresolved intensity centered on 8 ppm (^{1}H) (Figure

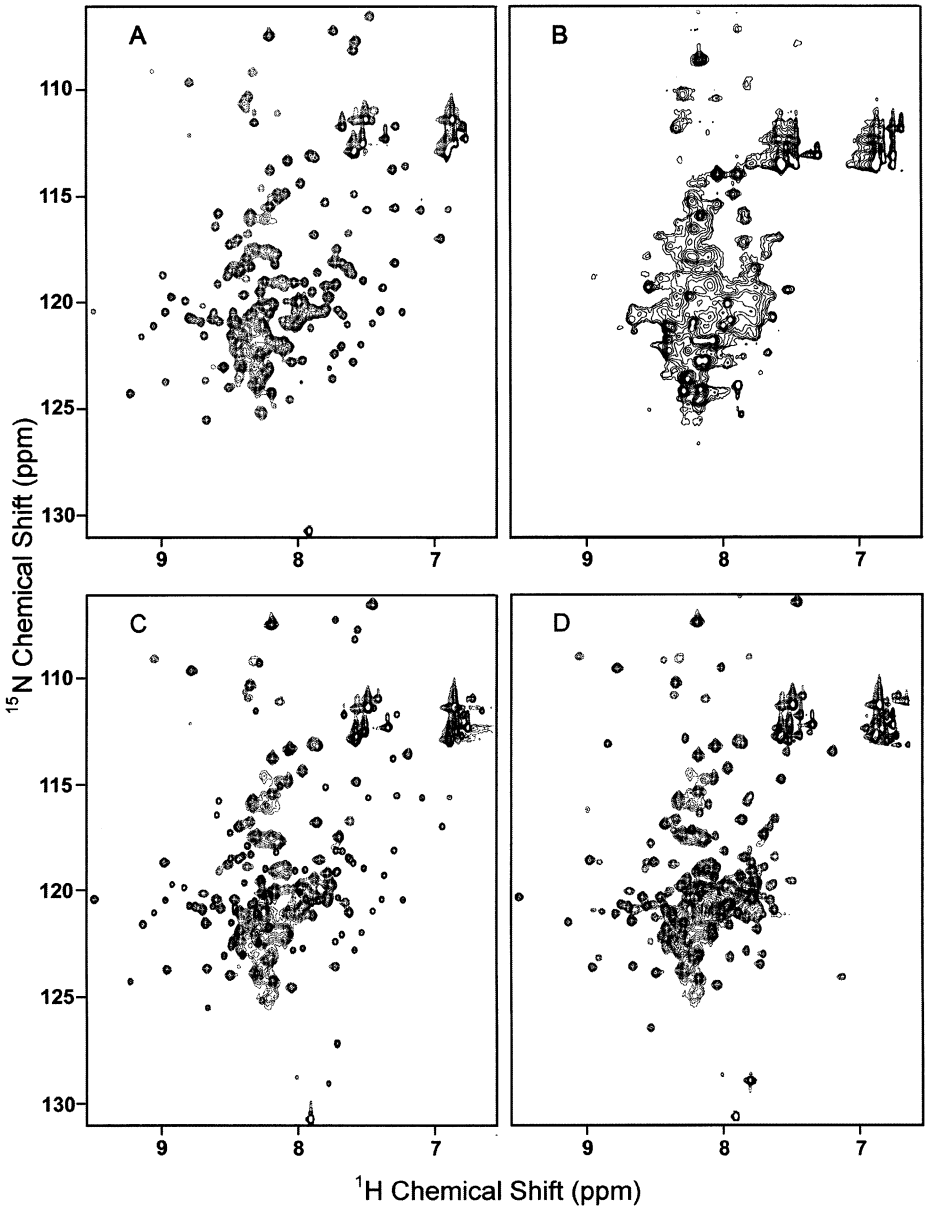

FIGURE 3: Interactions between 2D and 3D but not between 1D and 2D. [^{15}N-^{1}H]-HSQC NMR spectra of uniformly labelled RAP fragments. Panel A, fragment 1D-2D (1−215); panel B, fragment 2D-3D (93−323); panel C, superpositioning of spectra of fragments 1−112 and 93-215; and panel D, superpositioning of spectra of fragments 93−215 and 206−323.

4A). The dispersed narrow resonances corresponded in position and resolution with those present in the fragment 1−112 (Figure 2A), suggesting that in the intact protein, this extreme N-terminal domain retains its structure and has motion that is independent of the remainder of the molecule. In keeping with this, the spectrum of intact RAP was very similar to the sum of spectra of 1D and 2D-3D (Figure 4B). A spectrum of RAP was also recorded at a very much lower concentration (10 μM) (Figure 4C) to determine if the broadening was concentration dependent. This spectrum showed the same pattern of resolved resonances from the N-terminal domain and broad resonance intensity from the remainder of the protein as was present at much higher concentrations.

Sedimentation Equilibrium and Velocity Measurements. Sedimentation equilibrium measurements were carried out on intact RAP and on the fragments 1D, 2D, 3D, and 2D-3D. All of these species behaved as monomers, with excellent agreement between the MWs deduced from the experimental data fitted to a single, ideal component model and the MWs calculated from the primary structures (Table 2).

Sedimentation velocity measurements were also carried out on intact RAP. The distribution profile showed that the sample sedimented with a sedimentation coefficient of ~2.5S (data not shown). If RAP behaved as a monomeric 38 kDa globular protein, it would be expected to have a sedimentation coefficient of 6.0S. The much smaller value observed suggests that RAP must have a nonglobular structure. When modeled as a prolate ellipsoid, an axial ratio of 11:1 is required to give the observed sedimentation coefficient.

Fluorescence Emission Spectra of RAP and RAP Fragments. RAP contains five tryptophan residues, two in the N-terminal domain, two in the middle domain, and one in the C-terminal domain of the protein. Tryptophan emission spectra were recorded for the fragments 1−112, 93−215, 206−323, and 1−215, as well as for intact RAP (Figure 5A). The wavelength maximum for the emission spectrum of the first domain was 335 nm, consistent with partial surface

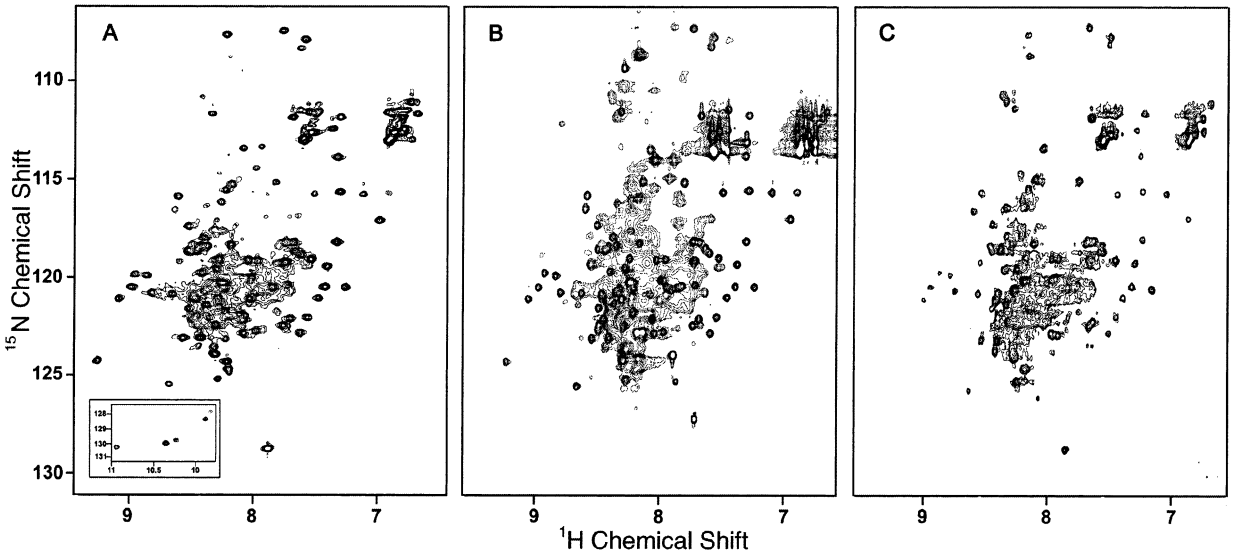

FIGURE 4: 2D-3D intact in intact RAP. Panel A, [^{15}N-^{1}H]-HSQC HSQC NMR spectrum of uniformly labelled RAP at 300 μM. The sharp, resolved resonances arise exclusively from domain 1D (compare to Figure 2A). Panel B, superpositioning of spectra of 1D (1−112) and 2D-3D (93−323) at 300 μM. Panel C, spectrum of intact RAP recorded at 10μM.

Table 2: Sedimentation Equilibrium of RAP and RAP Fragments

construct	experimental MW (Da)	calculated MW (Da)
1D (1−112)	12 400	12 947
2D (93−215)	12 280	14 270
3D (206−323)	12 670	12 705
2D-3D (93−323)	25 450	26 956
RAP (1−323)	37 430	37 769

exposure of both of the tryptophans, as found in the solution structure. A spectrum with a similar wavelength maximum, although lower intensity, was found for the 93−215 fragment. The emission spectrum of the final domain was about 50% of the intensity of the first domain and more intense than the middle domain, despite having only one tryptophan. In addition, the wavelength maximum was more red-shifted, to 342 nm, suggesting a more solvent exposed location than the average for the pairs of tryptophans in each of the other two domains. The spectrum of the larger fragment 1−215 was indistinguishable from that of a mixture of the 1−112 and 93−215 fragments in 1:1 ratio and was nearly an exact superpositioning of the spectra of the isolated 1−112 and 93−215 fragments (Figure 5B). Similarly, the spectrum of intact RAP was well-matched by the sum of spectra of the 1−215 fragment and the C-terminal 206−323 fragment (Figure 5C) and by the sum of the spectra of 1−112, 93−215, and 206−323 fragments (Figure 5D). The same was true if the spectra of 1:1 and 1:1:1 mixtures of these fragments, respectively, were compared (Figure 5C,D).

DISCUSSION

Prior to this study on the domain composition and organization of RAP, several quite different models had been proposed for RAP that involved the presence of two, three, or four domains (*12*, *14*, *16*). These models were mostly based on techniques that did not report directly on the tertiary structure of the constructs being examined. In the present study, we have used not only DSC, fluorescence, and sedimentation measurements but also much more structurally informative two-dimensional NMR spectroscopy to obtain a model that represents a much more detailed description of the domain organization of RAP and one that differs in one or more important respects from any of the previously published models.

Differential scanning calorimetric measurements of the constructs 1D, 2D, and 3D presented here showed that each of these species contains a discretely folded domain, with a well-defined unfolding temperature. The nearness of the $\Delta H^{\mathrm{cal}}/\Delta H^{\mathrm{van't\ Hoff}}$ ratio to a value of 1 for the unfolding transitions of each of these species supports the conclusion that each consists of only a single domain. Sedimentation equilibrium measurements furthermore showed that each domain remains monomeric as an isolated species. Importantly, two-dimensional NMR spectroscopy shows that each of these monomeric species contains a well-defined stable tertiary structure, although the extent of such a structure varies with the domain, being most extensive for 1D, less for 2D, and least for 3D. This is also the order of decreasing stability for these domains, indicated by the DSC unfolding temperature, suggesting a relationship between the stability of the domain and the extent of well-defined tertiary structure present.

Whereas one earlier model had also proposed the existence of three domains, based on the appearance of one-dimensional ^{1}H NMR spectra, that study did not examine the behavior of pairs of domains or compare the behavior of a given domain in isolation with its behavior in intact RAP (*12*). As a result, the model did not address how individual domains might interact with one another. In the present study, two-dimensional HSQC NMR spectra of 1D, of the tandem construct 1D-2D, and of intact RAP showed that 1D is completely independent of the remainder of the protein and is only loosely linked to domain 2D, thereby allowing it completely independent motion. In contrast, two-dimensional HSQC spectra of 2D and 3D, as isolated domains, as the tandem construct 2D-3D, or as part of intact RAP, showed that these domains interact with one another in the same way in both 2D-3D and intact RAP. Sedimentation velocity measurements on RAP, which was shown from separate sedimentation equilibrium measurements to be

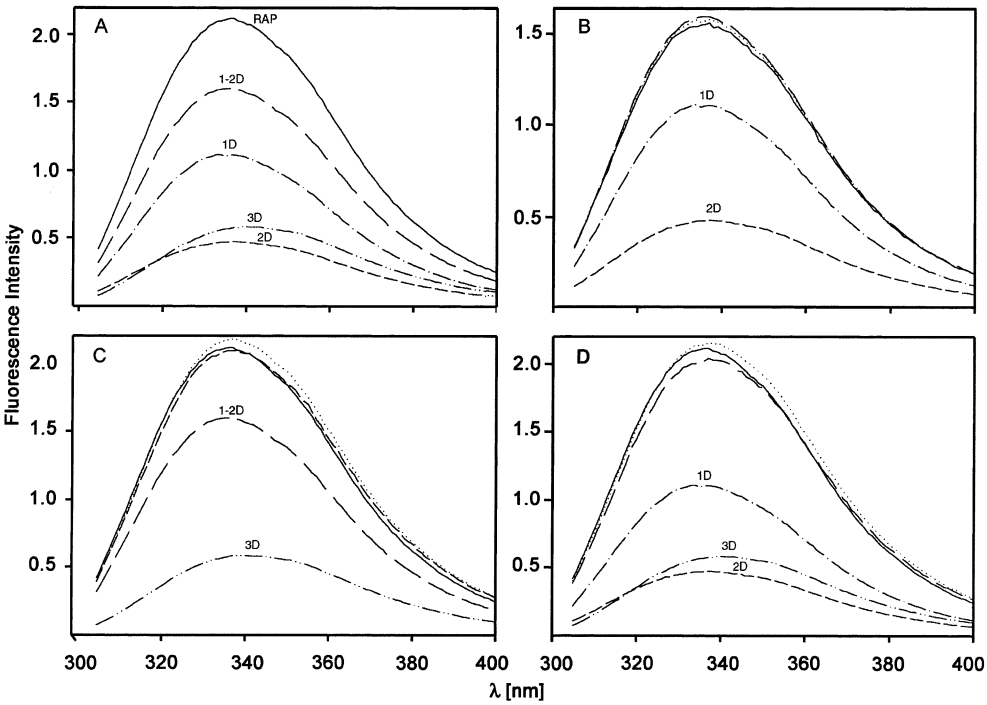

FIGURE 5: Tryptophans in different RAP domains do not interact with one another. Fluorescence emission spectra of RAP and RAP fragments. Panel A, dot−dashed line, 1D; dashed line, 2D; dot−dot−dashed, line 3D; long dashed line, 1−2D; and solid line, intact RAP. Panel B, dot−dashed line, 1D; dashed line, 2D; long dashed line, 1−2D; solid line, spectrum of a 1:1 mixture of 1D and 2D; and dotted line, calculated sum of spectra of 1D and 2D. Panel C, long dashed line, 1−2D; dot−dot−dashed line, 3D; dashed line, spectrum of a 1:1 mixture of 1−2D and 3D; solid line, RAP; and dotted line, calculated sum of spectra of 1−2D and 3D. Panel D, dot−dashed line, 1D; dashed line, 2D; dot−dot−dashed line, 3D; long dashed line, 1:1:1 mixture of 1D, 2D, and 3D; dotted line, calculated sum of spectra of 1D, 2D, and 3D; and solid line, RAP. Excitation was at 295 nm.

monomeric, gave a sedimentation coefficient that indicates that the protein must be nonglobular and highly elongated.

The present results, taken together, thus suggest a quite distinct new model for RAP of three domains of similar size, arrayed in an extended manner, with the first domain quite independent of the other two, and with the second and third domains interacting in a way that causes broadening of most or all of their resonances.

Nature of the Interaction between 2D and 3D. The present results do not permit an unambiguous description of the nature of the interaction of domains 2D and 3D to be obtained. Fluorescence measurements on isolated RAP domains, on tandem constructs, and on intact RAP suggest that there is no major conformational change that affects domains 2D and 3D when they are part of the same protein since the fluorescence spectra always appear to be additive. This could, however, also result either from compensatory changes that give the same final fluorescence intensity or from the limited number of reporter groups giving too local a perspective of the protein conformation. It is clear, however, from the dramatic increase in broad resonance intensity in the center of the two-dimensional HSQC NMR spectra of 2D-3D and intact RAP and loss of signal from the dispersed resonances as compared with the sums of isolated domains, that the interaction between 2D and 3D is not a tight association of the two domains to give one that effectively has twice the molecular weight. Such an interaction would lead to resonance broadening but would do so in a manner than resulted in an approximate doubling of line width for the dispersed resonances seen in the spectra of the isolated domains and perturbation of the chemical shift only for those that are at the contact interface. This is not what was observed. Instead, dramatic broadening and concomitant loss of spectral dispersion was observed that is more consistent with a weaker interaction in which there is an exchange between well-populated associated and dissociated conformations. Since this is an intramolecular process, it should be independent of RAP concentration, which is what was found for two-dimensional HSQC NMR spectra run at high and low concentrations. Such an exchange between closed and open conformations is also consistent with the sedimentation velocity measurements, which imply a quite elongated average structure for RAP.

Given the evidence from the present study for a three-domain structure for RAP, it is instructive to reexamine earlier alternative proposals of two (*16*) or four domains (*14*). The two-domain proposal acknowledged the likelihood that all secondary structural elements would be α-helical and that the three helical bundle found in the first 100 residues would be present in the final structure. In particular, the idea that RAP might be a two-domain protein came from the biphasic denaturation behavior of intact RAP toward guanidine hydrochloride followed by CD. The authors also found that only the regions from 15 to 94 and from 223 to 323 were largely resistant to proteolysis, suggestive of folded structures only within these regions. To accommodate a two-domain structure, as well as the different proteolytic susceptibility of the first and second halves of the middle repeat and the indication from binding studies that there might be an interaction between the first and the middle repeats, it was proposed that a predicted helix from 134 to 159 interacts tightly with the N-terminal three-helical bundle to give a domain containing four helices, while the second domain was suggested to be composed of one very long helix from

the C-terminal repeat interacting with two small helices, one each from the middle repeat (residues 185−196) and from the C-terminal repeat (residues 285−293). Our NMR results clearly show that domain 1D (residues 1−112) is independent of the remainder of the protein and thus cannot form part of a larger 4 helix bundle with part of the central repeat, while both 2D and 3D are well-structured domains in their own right.

The major differences between the present three-domain model and the four-domain model of Medved et al. (*14*) is the proposed presence of two domains (D2 and D3, residues 93−163 and 164−216, respectively) within the region corresponding to the middle domain of the present model (2D, residues 112−215), a proposed interaction between their first domain (D1) and their second domain (D2) and a proposal here that domains 2D and 3D interact. The proposed domain boundary between D2 and D3 occurs at 163−164, which is the start of a region containing several proteolytically sensitive sites found by Wardell and colleagues (*16*). The present NMR data, showing that 1D is independent of 2D, whether it is part of intact RAP or of the 1D-2D tandem repeat, are not compatible with the interaction between D1 and D2 of the four-domain model. In addition, the similarity of NMR spectra of constructs 1−112 and 1−164, as far as number and position of sharp, resolved resonances, is not consistent with the presence of a discrete well-structured domain encompassing residues 112−164. It is significant that the earlier study also examined by DSC constructs covering each of the regions that we propose to be discrete domains and found only a single well-defined unfolding transition for each. These were reproduced in the present study. Also significant was that the authors reported that it was not possible to obtain a stable construct for domain D3 (residues 164−216) and that the construct representing their domain D2 (residues 89−163) gave no unfolding transition by DSC (although it did give a small change in heat capacity and evidence from CD spectra for loss of α-helix over a wide temperature range). In contrast, the present DSC data strongly suggest only a single domain for each of the three repeats of the protein. In keeping with this, an explanation for the absence of a separate unfolding transition for the region 89−164 (although with a change in heat capacity) is that it represents premature termination of our central domain (2D). Such premature termination would disrupt the domain and make it unstable, even though there might still be high α-helical content. As the temperature is increased, this region would be expected to progressively lose its α-helical content and hence give rise to a small change in heat capacity. Also consistent with this, the remainder of this region, residues 165−215, would not be expected to have a stable tertiary structure, thus explaining the difficulty in preventing proteolytic degradation of this construct during expression and isolation.

ACKNOWLEDGMENT

We gratefully acknowledge the use of instruments in the Keck Biophysics Facility at Northwestern University (http://www.biochem.northwestern.edu/Keck/keckmain.html). We thank Dr. Francis Peterson for the expression vector pQE30NusA-TEV and Dr. Steven Olson for comments on the manuscript.

REFERENCES

1. Ashcom, J. D., Tiller, S. E., Dickerson, K., Cravens, J. L., Argraves, W. S., and Strickland, D. K. (1990) *J. Cell. Biol. 110*, 1041−1048.
2. Willnow, T. E., Rohlmann, A., Horton, J., Otani, H., Braun, J. R., Hammer, R. E., and Herz, J. (1996) *EMBO J. 15*, 2632−2639.
3. Bu, G., and Rennke, S. (1996) *J. Biol. Chem. 271*, 22218−22224.
4. Li, Y., Lu, W., Schwartz, A. L., and Bu, G. (2002) *Biochemistry 41*, 4921−4928.
5. Bu, G., Williams, S., Strickland, D. K., and Schwartz, A. L. (1992) *Proc. Natl. Acad. Sci. U.S.A. 89*, 7427−7431.
6. Nykjaer, A., Petersen, C. M., Moller, B. K., Jensen, P. H., Moestrup, S. K., Holtet, T. L., Etzerodt, M., Thøgersen, H. C., Munch, M., and Andreasen, A. M. (1992) *J. Biol. Chem. 267*, 14543−14546.
7. Orth, K., Madison, E. L., Gething, M.-J., Sambrook, J. F., and Herz, J. (1992) *Proc. Natl. Acad. Sci. U.S.A. 89*, 7422−7426.
8. Williams, S. E., Ashcom, J. D., Argraves, W. S., and Strickland, D. K. (1992) *J. Biol. Chem. 267*, 9035−9040.
9. Troussard, A. A., Khallou, J., Mann, C. J., André, P., Strickland, D. K., Bihain, B. E., and Yen, F. T. (1995) *J. Biol. Chem. 270*, 17068−17071.
10. Nielsen, P. R., Ellgaard, L., Etzerodt, M., Thogersen, H. C., and Poulsen, F. M. (1997) *Proc. Natl. Acad. Sci. U.S.A. 94*, 7521−7525.
11. Strickland, D. K., Ashcom, J. D., Williams, S., Battey, F., Behre, E., McTigue, K., Battey, J. F., and Argraves, W. S. (1991) *J. Biol. Chem. 266*, 13364−13369.
12. Ellgaard, L., Holtet, T. L., Nielsen, P. R., Etzerodt, M., Gliemann, J., and Thogersen, H. C. (1997) *Eur. J. Biochem. 244*, 544−551.
13. Pace, C. N., Vajdos, F., Grimsley, G., and Gray, T. (1995) *Protein Sci. 4*, 2411−2423.
14. Medved, L. V., Migliorini, M., Mikhailenko, I., Barrientos, L. G., Llinás, M., and Strickland, D. K. (1999) *J. Biol. Chem. 274*, 717−727.
15. Delaglio, F., Grzesiak, A., Vuister, G. W., Zhu, G., Pfeifer, J., and Bax, A. (1995) *J. Biomol. NMR 6*, 277−293.
16. Rall, S. C., Jr., Ye, P., Bu, G., and Wardell, M. R. (1998) *J. Biol. Chem. 273*, 24152−24157.

BI035779E